Supplementary Information

Less than 5 Netrin-1 molecules initiate attraction but 200 Sema3A molecules are necessary for repulsion

Giulietta Pinato[1+], Dan Cojoc[1*+], Linh Thuy Lien[2], Alessio Ansuini[2], Jelena Ban[2], Elisa D'Este[1] & Vincent Torre[2,3*]*

[1]Istituto Officina dei Materiali (IOM-CNR), Area Science Park, Basovizza, S.S. 14, Km 163.5, 34149 Trieste, Italy
[2]Neurobiology Sector, International School for Advanced Studies (SISSA), via Bonomea 265, 34136 Trieste, Italy
[3]IIT, Italian Institute of Technology, SISSA-Unit, Trieste, Italy

* correspondence: pinato@iom.cnr.it, torre@sissa.it, cojoc@iom.cnr.it
[+] equally contributed

Supplementary Information 1

The optical set-up

The optical setup (Supplementary Fig.1) is composed of three main modules [1]: custom built IR optical tweezers (Supplementary Fig.1, red box); commercial UV micro-dissection system (MMI-CellCut Plus, MMI, Zurich, Switzerland; Supplementary Fig.1, blue box); commercial inverted microscope Nikon Eclipse TE-2000-E (Supplementary Fig.1, yellow box). The trapping laser beam is generated by a 1064 nm continuous wave single mode Yb fibre laser (YLM-5, IPG Photonics GmbH, Burbach, Germany). The laser beam is expanded by a collimator (Supplementary Fig.1, L1) so to have a beam with a diameter Db= 15 mm, large enough to over-fit the entrance pupil (diameter Dp = 11 mm) of the objective lens (Nikon, 60x water immersion, numerical aperture (NA): 1.2, working distance (WD): 0.31 mm), thus meeting the conditions for an optimum trapping [2]. The 60x objective lens provides a good transmission from UV to IR light allowing simultaneous UV dissection, IR trapping and differential interference contrast (DIC) imaging.
The trapping IR beam is aligned with the micro-dissection UV beam by two mirrors (Fig. 8, M1 and M2). A convergent lens (Supplementary Fig.1, L2), with the focal length f = 150 mm is placed just before the entrance aperture of the micro-dissection to adjust the convergence of the trapping IR beam to the convergence of the UV micro-dissection beam. The power of the IR laser necessary to trap vesicles varied between 10 to 20 mW. The micro-dissection system is equipped with a solid-state pulsed UV laser (355 nm, max 1 μJ/pulse, pulse duration <0.5 ns, repetition rate <5 kHz). The beam is collimated by internal optics and directed to the microscope objective by two dichroic mirrors (Supplementary Fig.1, DM1 and DM2). The number of required pulses could vary with vesicle morphology (single or multi-lamellar) and 1–3 pulses are usually enough to break the vesicles.

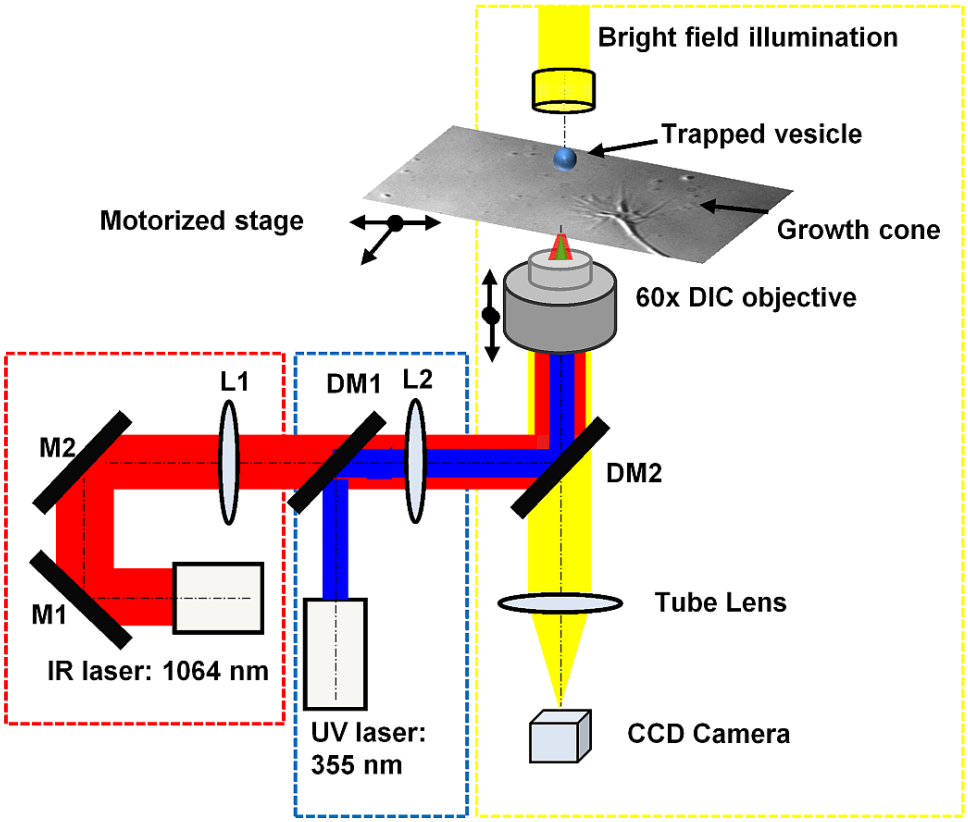

Supplementary Figure 1: Optical setup. The three modules composing the optical manipulation setup: IR optical tweezers (red); UV micro-dissection (blue); and the inverted microscope (yellow). The IR laser trapping beam direction is adjusted by two mirrors, M1 and M2, and it is expanded by the collimator L1. The convergent lens L2 adjusts the convergence of the IR beam to the convergence of the UV beam of the micro-dissection system. Both laser beams are then directed into the entrance pupil of the microscope objective (60X DIC) by the dichroic mirrors DM1 and DM2. The sample is illuminated by a white light source and the image is formed through the tube lens on the CCD camera.

Supplementary Information 2

Experimental determination of diffusion following vesicle breaking

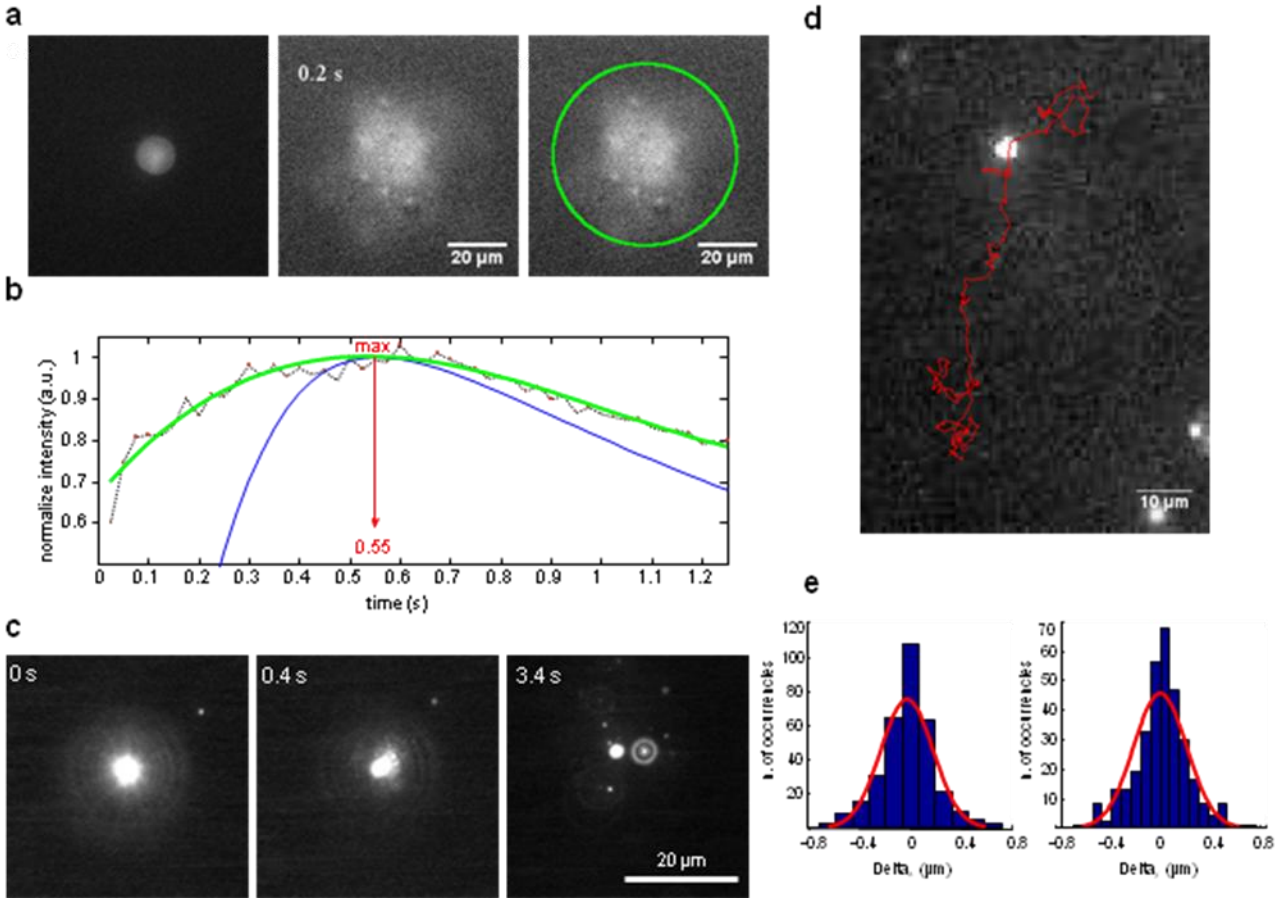

Supplementary Figure 2: Calibration of diffusion using imaging fluorescent molecules. (a) fluorescence image of a lipid vesicle filled with fluorescein and optically trapped (left panel). Images of the diffusion of fluorescein at t=0.2 s after photolysis (central and right panel). The green circle in the right panel reproduces a thin ring used to quantify the diffusion process (see text for further information). Raw images have been processed with histogram normalization to enhance contrast. **(b)** comparison of the time course of F(R,t) and P(R,t) (see text for further information). **(c)** fluorescence image of a lipid vesicle filled with QDs and optically trapped before photolysis (0 s) and during diffusion of QDs (0.4 s and 3.4 s) after photolysis. **(d)** single QD trajectory tracking. One frame, selected from a sequence of 331 frames taken in 16.5 s at 20 Hz, showing the QD (white spot) and its trajectory (red line). **(e)** probability distribution of the increments Δx and Δy of the QD position in consecutive frames.

We performed two types of diffusion experiments encapsulating fluorescein molecules and Quantum Dots (QDs) inside lipid vesicles and recording the fluorescence after vesicles photolysis with UV laser pulses.

Fluorescein (MW=332.3 Da, diffusion coefficient D=270 $\mu m^2 s^{-1}$) at 1 mM concentration was encapsulated in vesicles with a diameter of about 10 µm and vesicles were optically trapped. Fluorescein confined inside a trapped vesicle positioned at about 30 µm above the coverslip was observed and the emitted fluorescence was measured with a CCD camera (Supplementary Fig. 2a (left)). When the vesicle is broken with a UV laser pulse, fluorescein and the associated fluorescence diffuse in the surrounding medium (Supplementary Fig. 2a (centre)) in an almost isotropic way. Deviations from isotropic diffusion might be caused by the asymmetric position of the breaking point

on the vesicle membrane. Due to bleaching during vesicle photolysis we could not monitor the time evolution of fluorescein concentration inside the vesicles following the UV laser pulse. Experiments with QDs – which do not bleach – show that after UV pulses all trapped QDs freely diffuse.

In order to verify more quantitatively whether trapped molecules diffuse in the medium, as expected from a simple diffusive process, we measured and characterized changes of emitted fluorescence. Therefore, we measured the fluorescence intensity F(R,t) in rings with an internal radius R and an external radius R+ΔR centered on the lipid vesicle, as shown in the image on the right-hand side of panel a. Typical values of R and ΔR were 30 μm and 1 μm. F(R,t) was measured in images acquired at 40 Hz during 1.5 seconds after vesicle photolysis. The time course of F(R,t) is shown in panel b as red points fitted with a polynomial function of the third order (green line), from which we calculated the time taken to reach its maximum value, i.e. t_{mExp}. We computed also the expected probability function P(R,t) for particles diffusing from the center of the vesicle and reaching a circle with radius R at time t (blue line). The probability of reaching R in a time t (P(R,t)) for particles with the same diffusion coefficient of Fluorescein (D= 270 $\mu m^2 s^{-1}$) has the time course shown by the blue line (Supplementary Fig. 2b). The measured F(R,t) and the predicted P(R,t) reach their maximum value at approximately the same time around 0.55 s. The deviation between the red and the blue lines before they reach their maximum level – i.e. before 0.5 s – is caused by the physical dimension of the lipid vesicle, while P(R,t) was computed assuming a point source. The agreement between predicted t_{mTheor} for pure diffusion and the measured value of t_{mExp} was confirmed for different concentric rings with radii varying from 18 to 32 μm. These results allow us to conclude that also non-fluorescent molecules, such as Sema3A and Netrin-1, following vesicle photolysis will diffuse in the surrounding medium.

Due to a partial bleaching of Fluorescein during vesicle photolysis by the focused UV laser we could not monitor with precision its concentration inside the vesicle. Nevertheless, following the QD experiments (which do not bleach) we verified that UV pulses break completely the vesicle allowing all trapped molecules to freely diffuse. Indeed, we have also repeated these experiments with fluorescent QDs since their emission is not bleached by the UV laser pulses. We have used PEG coated QDs to avoid/reduce aggregation. In these experiments we could also follow the diffusion of single QDs. As shown in Supplementary Fig. 2c (left image), before the vesicle breaking the QDs fluorescence is confined within the lipid vesicle. After the UV pulse, QDs diffuse in the surrounding medium and individual QDs can be occasionally imaged (see central and right image Supplementary Fig. 2c). Since QDs diffuse in the 3D medium, their motion is not confined in the focal plane of the microscope and therefore they can disappear and reappear. Occasionally it was possible to follow for several seconds the trajectory of an individual QD as shown in Supplementary Fig. 2d. From the QD trajectory we computed the probability distribution of the increments Δx and Δy of its position in consecutive frames and as shown in Supplementary Fig. 2e, their distribution has a Gaussian profile as expected from a diffusive process. All these results, taken together, show that molecules trapped inside lipid vesicles, and after the UV pulse, diffuse in the surrounding medium following a diffusive dynamics in agreement with their diffusion coefficient *D*.

Supplementary Information 3

Computation of the distance between the vesicle and the closest neurite tip

A region of interest (ROI) - selected by the operator - containing the vesicle in front of the exploring GC is identified (Supplementary Fig. 3a, yellow polygon). The image is convolved with a battery of even directional filters and squared outputs of these filters are added (Supplementary Fig. 3b). This procedure enhances thin shapes, i.e. filopodia and thin neurites. The image in Supplementary Fig. 3b is binarized (Supplementary Fig. 3c) and thin shapes within the ROI are assumed to be filopodia emerging from the GC. The operator marked with a red cross the center of the vesicle and with a blue dot a point inside the GC. All lines starting from the blue dot and following the detected thin shapes are considered (Supplementary Fig. 3d, green lines); and the line with the shortest distance *Dist* between their tips and the red cross (Supplementary Fig. 3d, cyan line) is taken as the neurite tip closest to the vesicle. The obtained value of *Dist* is taken as the distance between the vesicle and the GC (Supplementary Fig. 3d).

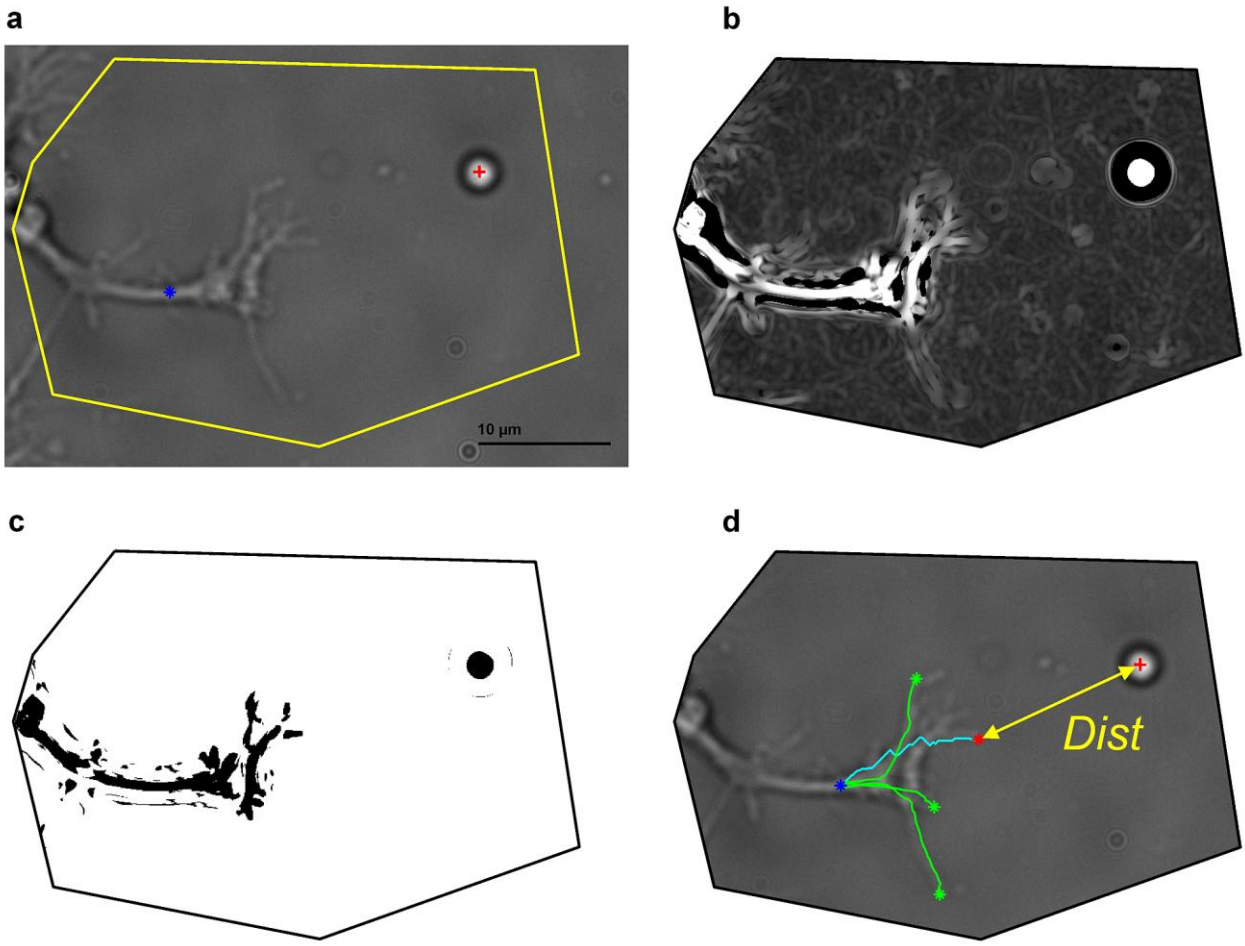

Supplementary Figure 3: Computation of the distance between the vesicle and the nearest filopodia tip. (a) an image of the GC and the trapped vesicle in front of it. In the initial image of the sequence, the experimenter defines the region of interest (ROI), by selecting a polygon (in yellow) and locates the GC by identifying a reference point inside the GC (blue dot) and the vesicle position L_v (red cross). **(b)** the image is convolved with a set of directional filters and the resulting outputs are squared and summed. **(c)** the resulting image is binarized. White thin shapes inside the ROI are identified as filopodia. **(d)** determination of *Dist*, as the shortest distance between the red cross and the identified filopodia.

Supplementary Information 4

Control experiments with local release of vehicle

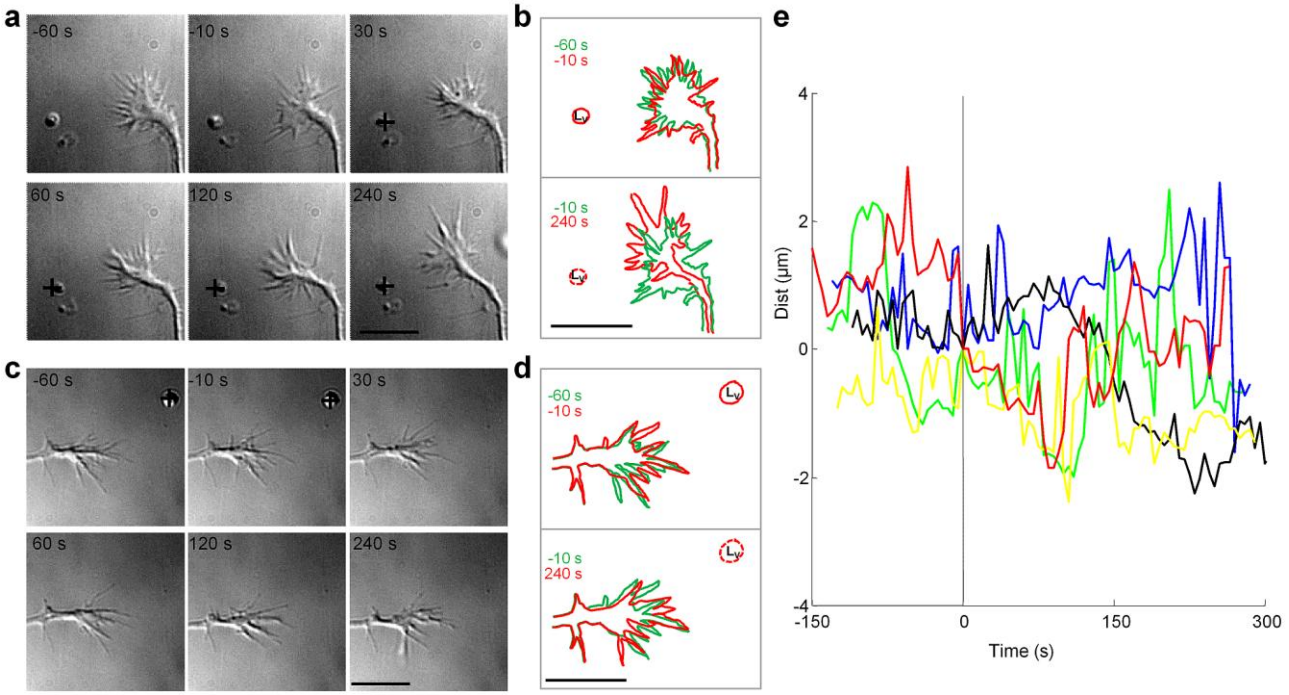

Supplementary Figure 4: Local release of vehicle from vesicles. (a) DIC images of a GC before VB (-60 s and -10 s) and after VB (30 s, 60 s, 120 s and 240 s). Black crosses indicate L_v. **(b)** top: GC profiles at -60 s (green) and -10 s (red) before VB ; bottom: GC profiles at -10 s (green) and 240 s (red) after VB. **(c)** as in a. **(d)** as in b but profiles obtained from the GC are shown in c. **(e)** time evolution of the distance (Dist) between L_v, i.e. the location of the center of the vesicle and the nearest tip of the GC for 5 different experiments. The vertical broken line indicates the time of VB. For these experiments vesicles were hydrated with PBS. Scale bar: 10 µm.

Supplementary Information 5

Immunostaining of Sema3A receptors in GC

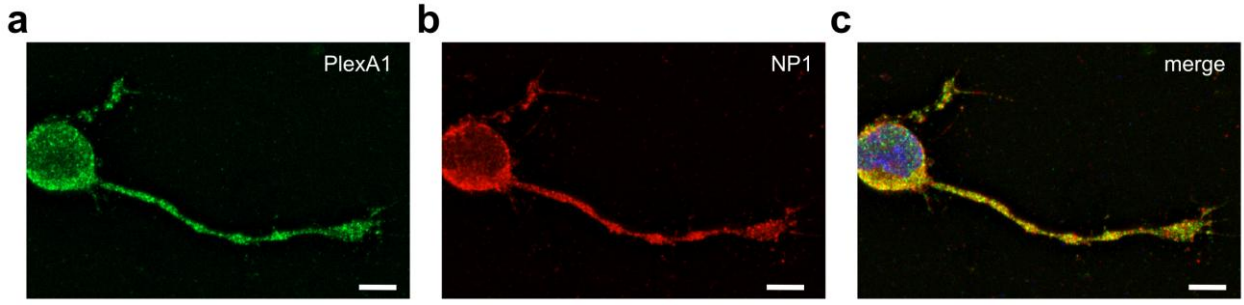

Supplementary Figure 5: **Sema3A receptors colocalize in hippocampal GCs**. **(a)** PlexinA1 (PlexA1, green), **(b)** neuropilin 1 (NP1, red) and **(c)** merged fluorescence image with nuclear staining (blue) of a hippocampal neuron after 16 hours of culture. The thresholded PCC (see Methods) is 0.67 indicating high degree of colocalization for the two Sema3A receptors. Scale bar = 10μm.

Supplementary Information 6

Immunostaining of UNC5A receptors in GC

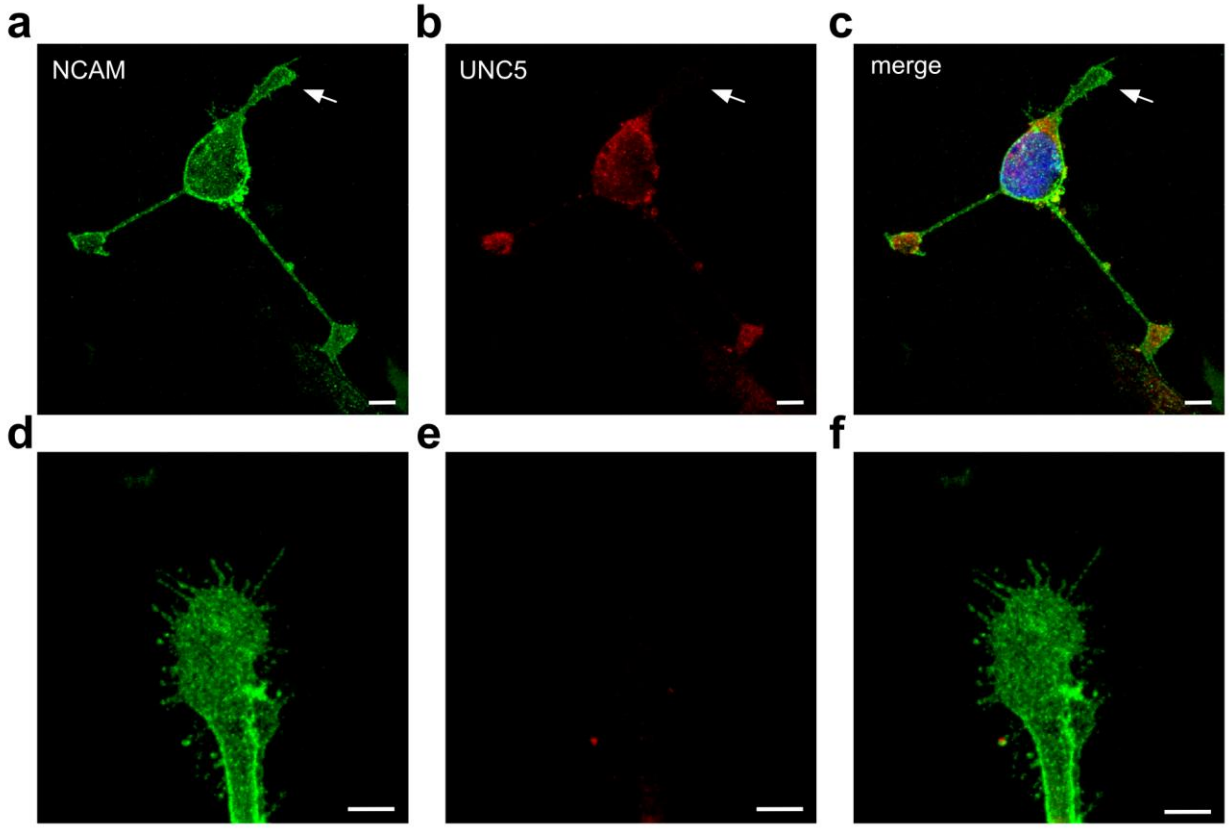

Supplementary Figure 6: UNC5A-negative GCs are observed without permeabilization. (a) and **(d)** Neural cell adhesion molecule (NCAM, green), **(b)** and **(e)** UNC5A (red), and **(c)** and **(f)** merged confocal fluorescence images. In the absence of Triton X-100, the overall expression of UNC5A decreased, in particular on neurites and GCs, but remained strong on the soma. Both UNC5A-positive and -negative GCs were found, sometimes also on the same neuron (see arrow in a-c that indicates a UNC5A-negative GC). In these experiments, half of the GCs were UNC5A-negative (d-f). Scale bar = 5μm.

Supplementary Information 7

Cytoplasmic localization of UNC5A receptors

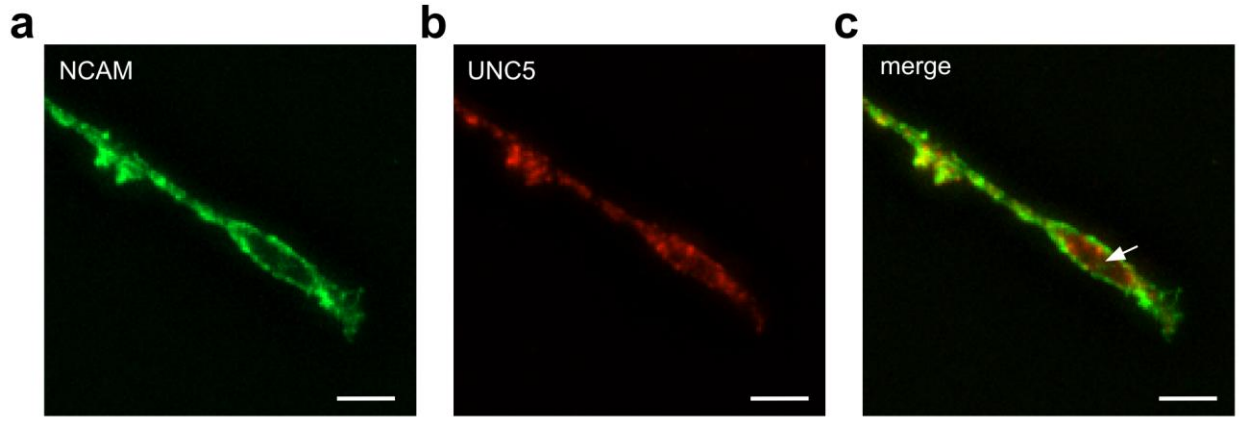

Supplementary Figure 7: Membrane and cytoplasmic localization of UNC5A receptors. (a) NCAM (green), **(b)** UNC5A (red) and **(c)** merged fluorescence images. The arrow in c indicates the cytoplasmic localization of UNC5A. Triton X-100 was used in the immunofluorescence protocol and all GC's were UNC5A-positive (more than 200 cells per coverslip analyzed in three independent experiments) indicating both membrane and cytoplasmic localization of UNC5A receptors. Scale bar = 5μm.

Supplementary Information 8

Estimation of the diffusion coefficient of Sema3A and Netrin-1

In order to estimate the diffusion coefficient *D* for Sema3A and Netrin-1, we looked for experimentally determined diffusion coefficients of proteins with a MW similar to Netrin-1 and Sema3A [3-5] . The MW of Sema3A is 65 kDa and of Netrin-1 is 75 kDa. The following table reports the diffusion coefficients experimentally determined D_{exp} for proteins with a MW ranging from 12.0 to 145.2 kDa.

Name	MW (kDa)	D_{sim} ($\mu m^2\ s^{-1}$)	D_{exp} ($\mu m^2\ s^{-1}$)
Cytocrome C	12.0	117	130
Ribonuclease A	13.8	98	107
Lysozyme	14.3	109	111
Myoglobin	17.9	102	108
Chymotrypsinogen	25.7	93	93
Sema3A	65.0	50.4	***
Malate dehydrogenase	74.3	60.9	57.6
Lactate dehydrogenase	145.2	49.6	50.5

Supplementary Table 1

The value of D_{exp} varies from 130 to 50.5 $\mu m^2\ s^{-1}$. In order to estimate the diffusion coefficient of Sema3A we used the program Hydropro [5, 6] which is a powerful tool to derive several hydrodynamic properties of molecules from their crystalline structure. The structure is encoded in .pdb (or .ent) files, available online at the RCSB PROTEIN DATA BANK (http://www.rcsb.org/pdb/home/home.do). The accuracy of Hydropro has been tested [5]. In order to calibrate the parameters required by Hydropro (water temperature, viscosity, protein MW, partial specific volume), we compared the estimated diffusion coefficients (D_{sim}) of several proteins in the considered range with the available experimental data [3-5] finding a very good agreement (see Supplementary Table 1).
The experimental value of the diffusion coefficient of Sema3A obtained from the Hydropro program is 50.4 $\mu m^2\ s^{-1}$, which is close to our previous estimate obtained with the Stokes formula ($D_{Stokes} = k_bT/6\pi\eta r$ =51 $\mu m^2\ s^{-1}$, where r is the radius of a sphere with the same MW of Sema3A). The crystalline structure of Netrin-1 is not available but a former estimate of its diffusion coefficient [7] was 40 $\mu m^2\ s^{-1}$, based on the typical scaling of the diffusion coefficient on MW. From these data the diffusion coefficient for Netrin-1 and Sema3A is expected to fall in the range [40-120] $\mu m^2\ s^{-1}$.

Supplementary Information 9

Analytical solution of the diffusion equation following vesicle breaking

When guidance molecules are released from the vesicle following the UV pulse, they diffuse in the surrounding medium. We use a reference system with the (x,y) plane coinciding with the dish, so that the location of the releasing vesicle is L_v *(0,0,a),* where *a* is the height of the vesicle from the bottom of the dish. The temporal evolution of the concentration follows the diffusion equation

$$\frac{\partial c}{\partial t} = D\,\Delta c \qquad (1S9)$$

where *c* is the concentration of guidance molecules and *D* is their diffusion coefficient. The initial condition is $c(\mathbf{x},0) = N_v\,\delta(\mathbf{x}-L_v)$, with N_v the total amount of guidance molecules inside the vesicle at time 0. The general solution of the equation (1S2) is

$$c(x,y,z,t) = \frac{1}{(4\pi Dt)^{3/2}} e^{-\frac{x^2+y^2+(z-a)^2}{4Dt}} \qquad (2S9)$$

In our case, the glass over which hippocampal neurons are located is impenetrable to guidance molecules and therefore diffusion occurs only in the half space $z > 0$. There are two main cases[8]:

- absorbing boundary conditions, i.e. particles arriving at the plane $z=0$ are trapped and absorbed

- reflecting boundary conditions, i.e. particles arriving at the plane $z=0$ are reflected and bounce back

The solution of the diffusion equation in the half space with absorbing boundary conditions is

$$c(x,y,z,t) = \frac{1}{(4\pi Dt)^{3/2}} e^{-\frac{x^2+y^2+(z-a)^2}{4Dt}} - \frac{1}{(4\pi Dt)^{3/2}} e^{-\frac{x^2+y^2+(z+a)^2}{4Dt}} \qquad (3S9)$$

The solution of the diffusion equation in the half space with reflecting boundary conditions is

$$c(x,y,z,t) = \frac{1}{(4\pi Dt)^{3/2}} e^{-\frac{x^2+y^2+(z-a)^2}{4Dt}} + \frac{1}{(4\pi Dt)^{3/2}} e^{-\frac{x^2+y^2+(z+a)^2}{4Dt}} \qquad (4S9)$$

Supplementary Information 10

Estimation of the number of molecules reaching the GC membrane for large values of the diffusion coefficient D

The mean square displacement $\langle x^2 \rangle$ of diffusing molecules is related to the diffusion coefficient D by:

$$\langle x^2 \rangle = q_i \, D t \qquad (1S10)$$

Where q_i is equal to 2,4 and 6 for 1,2 and 3-dimensional diffusion ($q_i = 2n$ where n is the dimension of the space in which the diffusion takes place). For proteins in water the range of D is [9]

$10^{-8} cm^2 s^{-1} < D < 10^{-6} cm^2 s^{-1}$ or $\mu m^2 s^{-1} < D < 10^2 \mu m^2 s^{-1}$

Therefore in 1s the order of magnitude of $\langle x^2 \rangle$ varies between 1 and 100 μm, and guidance molecules released from a vesicle at 4-6 μm from the GC could remain in its proximity for several seconds wandering around it. If D is larger than 10^4 μm^2 s^{-1}, on the timescale of 1s the trajectories become close to straight lines and their average displacement is larger than 1 μm.

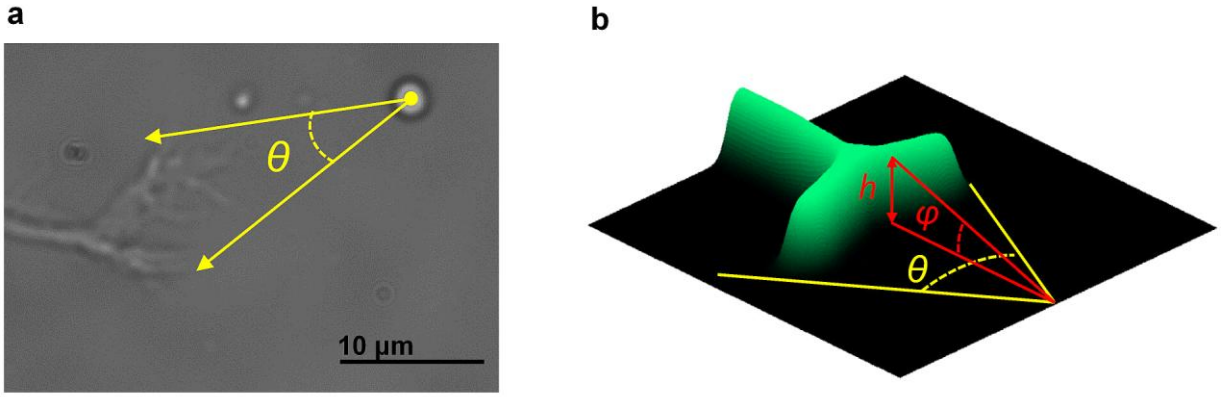

Supplementary Figure 10: Computation of the solid angle spanned by the GC. (a) An image of the GC and of the trapped vesicle. The experimenter defines the center of the vesicle and identifies the azimutal angle θ from which the GC is viewed by an observer assumed to be located at the center of the vesicle. **(b)** The zenith angle φ depends on the estimated thickness *h* of the GC.

Under these conditions, the number of molecules reaching the GC is approximately:

$$N_{GC} = N_v \Omega_{GC} / 4\pi \qquad (2S10)$$

where Ω_{GC} is the solid angle subtended by the GC assuming the observer is located at the center of the vesicle (Supplementary Fig. 10b). Simple geometrical considerations show that

$$\Omega_{GC} = (1 - \cos\theta)\, \varphi \qquad (3S10)$$

where $\varphi = \arcsin(\Delta z / Dist)$, Δz is the GC height, *Dist* is the distance from the vesicle and θ is the angle spanning the GC in the (x,y) plane when viewed from the vesicle (see Supplementary Fig. 10a). Assuming that Δz is 200 nm the ratio N_{GC}/N_v has values around 1%.

References

1. Pinato, G. et al. Neuronal chemotaxis by optically manipulated liposomes. *J Europ. Opt. Soc. Rap. Public.* **6**, 11042
(2011)
2. Neuman, K. C. and Block, S. M. Optical trapping. *Rev Sci Instrum* **75**, 2787-809 (2004)
3. Creighton, T. E. *Proteins: structures and molecular properties*. W.H. Freeman, 1993
4. Brune, D. and Kim, S. Predicting protein diffusion coefficients. *Proc Natl Acad Sci U S A* **90**, 3835-9 (1993)
5. Garcia De La Torre, J., Huertas, M. L. and Carrasco, B. Calculation of hydrodynamic properties of globular proteins from their atomic-level structure. *Biophys J* **78**, 719-30 (2000)
6. Ortega, A., Amoros, D. and Garcia de la Torre, J. Prediction of hydrodynamic and other solution properties of rigid proteins from atomic- and residue-level models. *Biophys J* **101**, 892-8 (2011)
7. Goodhill, G. J. Diffusion in axon guidance. *Eur J Neurosci* **9**, 1414-21 (1997)
8. Crank, J. *The mathematics of diffusion*. Clarendon Press, Oxford 1975
9. Howard, J. *Mechanics of motor proteins and the cytoskeleton*. Sinauer Associates, Publishers, 2001